Journal of Chemistry and Technologies, 2025, *33*(2), 558-569

Journal of Chemistry and Technologies

pISSN 2663-2934 (Print), ISSN 2663-2942 (Online).

journal homepage: http://chemistry.dnu.dp.ua
editorial e-mail: chem.dnu@gmail.com

UDC 519.63:532.5

NUMERICAL STUDY OF DOUBLE CATTANEO-CHRISTOV DIFFUSION EFFECTS IN MHD 3-DIMENSIONAL CASSON FLUID FLOW PAST AN EXPONENTIALLY STRETCHING SHEET

Suresh Pallerla[1], Javvaji Venkata Madhu[2], Nagaraju Bathula[3], Gundagani Murali[4*]

[1]*Department of Mathematics, Chaitanya Bharathi Institute of Technology, Hyderabad, India.*
[2]*Department of Mathematics, Sreenidhi Institute of Science and Technology, Yamnampet, India.*
[3]*Department of Mathematics, Palamuru University, Mahbubnagar, India.*
[4]*Department of Mathematics, Geethanjali college of Engineering and Technology, Cheeryal, Hyderabad, India.*
Received 24 November 2024; accepted 29 March 2025; available online 15 July 2025

Abstract

A numerical study of a three-dimensional steady-state flow of a viscous incompressible Casson fluid containing nanofluid particles interacting with a stretching sheet is the primary focus of this work. The equations for concentration and energy include the Cattaneo-Christov double diffusion effects. The Prandtl number plays a crucial role in assessing heat transfer characteristics in fluids. Within nanofluid dynamics, Brownian motion and thermophoresis significantly influence thermal behavior. The Cattaneo-Christov double-diffusion model extends traditional energy and concentration equations by incorporating thermal and solutal relaxation times. Transforming partial differential equations into ordinary differential equations is achieved through appropriate similarity variables. Numerical solutions are obtained using the finite element method to analyze modified governing equations. Graphical representations illustrate the impact of key parameters on velocity, temperature, and concentration profiles. Additionally, computational results evaluate skin friction, Nusselt number, and Sherwood number to quantify heat and mass transfer rates. These insights contribute to advancements in thermal engineering and nanofluid research, offering valuable applications for scientists and engineers working on enhanced heat transfer systems.

Keywords: three dimensional; exponentially stretching sheet; Casson fluid; magnetic field; nanofluid; Cattaneo-Christov double diffusion: Finite element method.

ЧИСЕЛЬНЕ ДОСЛІДЖЕННЯ ЕФЕКТІВ ПОДВІЙНОЇ ДИФУЗІЇ КАТТАНЕО-ХРІСТОВА В MHD D-ТРИВИМІРНІЙ ТЕЧІЇ КАССОННОЇ РІДИНИ ПОВЗ ЕКСПОНЕНЦІАЛЬНО РОЗТЯГНУТУ ПЛАСТИНУ

Суреш Палерла[1], Джавваджі Венката Мадху[2], Нагараджу Батхула[3], Гундаґані Муралі[4*]

[1]*Кафедра математики, Технологічний інститут Чайтанья Бхарті, Хайдарабад, Індія.*
[2]*Кафедра математики, Науково-технологічний інститут Срініджі, Ямнампет, Індія.*
[3]*Кафедра математики, Університет Паламуру, Махбубнаґар, Індія.*
[4]*Кафедра математики, Інженерно-технологічний коледж Гітанджалі, Чірувал, Хайдарабад, Індія.*

Анотація

Основна увага в цій роботі приділена чисельному дослідженню тривимірної стаціонарної течії в'язкої нестисливої рідини Кассона, що містить наночастинки, які взаємодіють з розтягнутою пластиною. Рівняння для концентрації та енергії включають ефекти подвійної дифузії Каттанео-Христова. Число Прандтля враховується при аналізі теплообмінних властивостей рідин. У нанорідинах важливу роль відіграють явища броунівського руху та термофорезу. Модель Каттанео-Крістова подвійної дифузії розширює класичні рівняння енергії та концентрації, враховуючи час теплової та солютальної релаксації. Система диференціальних рівнянь у частинних похідних перетворюється на звичайні диференціальні рівняння за допомогою спеціальних перетворень. Для чисельного розв'язання використовується метод скінченних елементів. Графічний аналіз демонструє вплив різних параметрів на швидкість, температуру та концентрацію. Додатково досліджуються коефіцієнти тертя, число Нуссельта та число Шервуда для оцінки ефективності тепло- і масообміну. Отримані результати можуть бути корисними для науковців та інженерів, які працюють із покращеними системами теплопередачі на основі нанорідин.

Ключові слова: тривимірний; експоненціально розтягнутий лист; рідина Кассона; магнітне поле; нанорідина; подвійна дифузія Каттанео-Крістова: метод скінченних елементів.

**Corresponding author: e-mail: muraligundagani@gmail.com*

doi: 10.15421/jchemtech.v33i2.314887

Introduction

Stretching-induced flows play an important part in industrial manufacturing, influencing the production of polymers and rubber as well as annealing and thinning of copper wire, cooling of spinning fiber, and extrusion from dye or polymer filaments. These flows are not just mechanical phenomena but are integral to the desired properties and performance characteristics of the materials. Furthermore, the application of fluid dynamics extends beyond these processes, as evidenced by the operation of heat exchangers, the technique of crop freezing, the design of air conditioning systems, the efficiency of solar power collectors, the functionality of cooling towers, and the innovation in desalination technologies.

Each of these examples demonstrates how fluid flows are important for heat and mass transfer and highlights the importance of understanding and optimizing the processes involved. By applying magnetohydrodynamics to a bidirectional stretching sheet, Nadeem and Lee [1] were able to obtain a simplified solution to clarify the boundary layer flow using a series solution. Sadiq et al. [2] examined the properties of an MHD unstable Nano fluid on a developing and shrinking boundary with convective condition. Akbar et al., [3] established a magnetohydrodynamic two-fold diffusion nanofluid flow over a stretched surface. Hussain and his colleagues studied the behaviour of the Reynolds number on the flow of a nanofluid over a stretching sheet with an overshoot. Ali et al. [5] conducted a study in a porous surface which is bidirectional and has a phase change, for studying heat and mass transfer. A number of authors [6–9] and [10] examined the effects of various fluid flows across a stretched sheet using numerical and analytical solutions. Resulting from a temperature difference, heat can be transferred between two objects or even within the same one. In formulating his revolutionary law, Fourier relied heavily on the idea of heat transmission, commonly referred to as "Fourier's law of heat conduction." This fundamental formula, while undeniably significant, falls short in providing a comprehensive representation of the intricate mechanisms governing heat transfer. These qualities include the immediate detection of any initial disturbance across the whole material. In actual application, there is no single object that can satisfy the criteria of Fourier's law. Cattaneo [11] included thermal relaxation into the conventional Fourier's law to resolve this problem. This suggests that heat transfer is comparable to the transmission of thermal waves traveling at a standard velocity. The Fourier heat equation and Cattaneo's equation are two instances of parabolic energy equations; the latter is a hyperbolic version of the former. Ciarletta and Straughan [12] used Cattaneo-Christov theory to explain the system's structure and how stable it is. The effect of Cattaneo-Christov heat flux on a Newtonian fluid experiencing thermal convection within a Maxwell fluid was studied by Mustafa [13] and Straughan [14]. Han et al. [15] reported their results on heat transmission in viscoelastic fluid flow using the Cattaneo-Christov model. Articles [16–19], and [20] provide some instances of potential uses. Numerous significant investigations undertaken in this domain are included in the references [21–44].

Examining the nanofluid is the driving force behind this project domain that is affected by thermophoresis, Brownian motion, magnetic fields, and Casson fluid particles on an exponentially expanding surface in three-dimensional orientations. This work is based on earlier research that has been published. Cattaneo-Christov heat flow effects are used to study how heat relaxation time affects fluid temperature, boundary layer thickness, and heat transfer coefficient. While looking at the model, we made a list of all its physical qualities. This was done before we looked at the physical properties of the problem. We used the basic equations and fundamental principles to construct a problem that includes the Cattaneo-Christov heat flux as well as magnetohydrodynamic effects. The basic partial derivative equations of the model are highly nonlinear and have been transformed into a dimensionless form using similarity transformations. This study uses a computer method for assessment, using the finite element methodology. We have conducted a visual study of the effect of different dimensionless components on the flow field using graphical representations. These physical parameters, such as Nusselt number and skin friction coefficient, we quantified and presented.

Calculation part

Flow Governing Equations:

In this paper, we investigate the three-dimensional flow behaviour of an incompressible, viscous and electrically conducting Casson fluid. This investigation incorporates Brownian motion, thermophoresis, nanofluid particles, magnetic field, and porous media. A thorough examination of the interplay between these factors is conducted in order to elucidate their cumulative impact on the fluid flow characteristics.

Journal of Chemistry and Technologies, 2025, *33*(2), 558-569

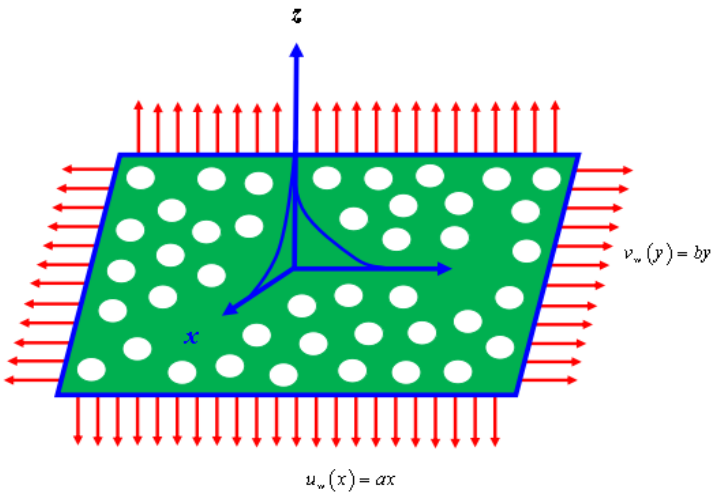

Fig. 1. Physical representation of Casson-Nanofluid flow

The physical configuration of the fluid flow for this inquiry is shown in Fig. 1. In accordance with established methodologies, the following key assumptions have been made to ensure the validity and reliability of the research findings. These assumptions are based on a thorough review of the existing literature and are deemed essential for the successful execution of this study.

a) Let (u, v, w) be the velocity components along the (x, y, z) directions, respectively.
b) Flow is generated due to an exponentially stretching surface.
c) A uniform magnetic field of strength B_0 is applied in the z – direction.
d) Magnetic Reynolds number is assumed very small so that the induced magnetic field is ignored.
e) The effects of double diffusion Cattaneo-Christov heat and mass fluxes are considered in energy and concentration equations respectively.
f) The characteristics of Brownian motion and thermophoresis are accounted.
g) The effects of Soret and Dufour are neglected in energy and concentration equations respectively.
h) The effects of viscous dissipation and joule heating are neglected in energy equation.
i) The effect of chemical reaction is neglected in concentration equation.
j) The rheological equation for a non-Newtonian fluid is defined as

$$\tau = \tau_o + \mu\alpha^* \tag{1}$$

Eq. (1) can be expanded for Casson fluid as,

$$\tau_{ij} = \begin{cases} 2\left(\mu_B + \dfrac{p_y}{\sqrt{2\pi}}\right)e_{ij}, & \pi > \pi_c \\ 2\left(\mu_B + \dfrac{p_y}{\sqrt{2\pi_c}}\right)e_{ij}, & \pi < \pi_c \end{cases}, \tag{2}$$

where $\pi = e_{ij}e_{ji}$ with e_{ij}

In the realm of scientific inquiry, these equations serve as the cornerstone, providing a framework for understanding and predicting the behavior of the systems under investigation. The intricate interplay between mass, momentum, energy, and nanoparticle concentration is encapsulated within these equations, offering valuable insights into the complex dynamics that govern such systems. In the context of the aforementioned assumptions, the fundamental equations governing mass conservation, momentum conservation, energy conservation, and nanoparticle concentration conservation are formulated as follows:

Continuity Equation:

$$u_x + v_y + w_z = 0 \tag{3}$$

Momentum Equation:

$$u\left(\frac{\partial u}{\partial x}\right) + v\left(\frac{\partial u}{\partial y}\right) + w\left(\frac{\partial u}{\partial z}\right) = \nu\left(1 + \frac{1}{\beta}\right)\left(\frac{\partial^2 u}{\partial z^2}\right) - \left(\frac{\nu}{k^*}\right)u - \left(\frac{\sigma B_o^2}{\rho}\right)u \tag{4}$$

Journal of Chemistry and Technologies, 2025, *33*(2), 558-569

$$u\left(\frac{\partial v}{\partial x}\right)+v\left(\frac{\partial v}{\partial y}\right)+w\left(\frac{\partial v}{\partial z}\right)=\nu\left(1+\frac{1}{\beta}\right)\left(\frac{\partial^2 v}{\partial z^2}\right)-\left(\frac{\nu}{k^*}\right)v-\left(\frac{\sigma B_o^2}{\rho}\right)v \tag{5}$$

Equation of thermal energy:

$$u\left(\frac{\partial T}{\partial x}\right)+v\left(\frac{\partial T}{\partial y}\right)+w\left(\frac{\partial T}{\partial z}\right)=\alpha\left(\frac{\partial^2 T}{\partial z^2}\right)+\tau_1\left\{D_B\left(\frac{\partial T}{\partial z}\right)\left(\frac{\partial \varphi}{\partial z}\right)+\frac{D_T}{T_\infty}\left(\frac{\partial T}{\partial z}\right)^2\right\}$$
$$-\gamma_1\left(\begin{array}{l} u^2\frac{\partial^2 T}{\partial x^2}+v^2\frac{\partial^2 T}{\partial y^2}+w^2\frac{\partial^2 T}{\partial z^2}+\left(u\frac{\partial u}{\partial x}+v\frac{\partial u}{\partial y}+w\frac{\partial u}{\partial z}\right)\frac{\partial T}{\partial x} \\ \left(u\frac{\partial v}{\partial x}+v\frac{\partial v}{\partial y}+w\frac{\partial v}{\partial z}\right)\frac{\partial T}{\partial y}+\left(u\frac{\partial w}{\partial x}+v\frac{\partial w}{\partial y}+w\frac{\partial w}{\partial z}\right)\frac{\partial T}{\partial z} \\ +2uv\frac{\partial^2 T}{\partial x\partial y}+2vw\frac{\partial^2 T}{\partial y\partial z}+2uw\frac{\partial^2 T}{\partial x\partial z} \end{array}\right) \tag{6}$$

Equation of species concentration:

$$u\left(\frac{\partial \varphi}{\partial x}\right)+v\left(\frac{\partial \varphi}{\partial y}\right)+w\left(\frac{\partial \varphi}{\partial z}\right)=D_B\left(\frac{\partial^2 \varphi}{\partial z^2}\right)+\frac{D_T}{T_\infty}\left(\frac{\partial T}{\partial z}\right)^2$$
$$-\gamma_2\left(\begin{array}{l} u^2\frac{\partial^2 \varphi}{\partial x^2}+v^2\frac{\partial^2 \varphi}{\partial y^2}+w^2\frac{\partial^2 \varphi}{\partial z^2}+\left(u\frac{\partial u}{\partial x}+v\frac{\partial u}{\partial y}+w\frac{\partial u}{\partial z}\right)\frac{\partial \varphi}{\partial x} \\ \left(u\frac{\partial v}{\partial x}+v\frac{\partial v}{\partial y}+w\frac{\partial v}{\partial z}\right)\frac{\partial \varphi}{\partial y}+\left(u\frac{\partial w}{\partial x}+v\frac{\partial w}{\partial y}+w\frac{\partial w}{\partial z}\right)\frac{\partial \varphi}{\partial z} \\ +2uv\frac{\partial^2 \varphi}{\partial x\partial y}+2vw\frac{\partial^2 \varphi}{\partial y\partial z}+2uw\frac{\partial^2 \varphi}{\partial x\partial z} \end{array}\right) \tag{7}$$

The boundary conditions for this flow are

$$\left.\begin{array}{l} u=u_w(x)=ax,\ v=v_w(y)=by,\ T=T_w,\ \varphi=\varphi_w\ at\ z=0 \\ u\to 0,\ v\to 0,\ T\to T_\infty,\ \varphi\to\varphi_\infty\ as\ z\to\infty \end{array}\right\} \tag{8}$$

Introducing the following similarity transformations

$$\left.\begin{array}{l} u=a(x+y)f'(\eta),\ v=b(x+y)g'(\eta),\ w=-\sqrt{a\nu}\left\{f(\eta)+Cg(\eta)\right\}, \\ \eta=\left(\sqrt{\frac{a}{\nu}}\right)z,\ \theta=\frac{T-T_\infty}{T_w-T_\infty},\ \phi=\frac{\varphi-\varphi_\infty}{\varphi_w-\varphi_\infty} \end{array}\right\} \tag{9}$$

Continuity equation is satisfied by Eq. (9) and Eqs. (4) to (7) will be of the below form

$$\left(1+\frac{1}{\beta}\right)f'''+ff''+gf''-f'^2-(M+\lambda)f'=0 \tag{10}$$

$$\left(1+\frac{1}{\beta}\right)g'''+fg''+gg''-g'^2-(M+\lambda)g'=0 \tag{11}$$

$$\theta''+\Pr f\theta'+\Pr g\theta'+\Pr Nb\theta'\phi'+\Pr Nt\theta'^2-\Pr Nb\gamma\left\{(f+g)^2\theta''+(f+g)(f'+g')\theta'\right\}=0 \tag{12}$$

$$Nb\phi''+NbScf\phi'+NbScg\phi'+Nt\theta''-NbSc\delta\left\{(f+g)^2\phi''+(f+g)(f'+g')\phi'\right\}=0 \tag{13}$$

The matching boundary conditions (8) transform into

$$\left.\begin{array}{l} f(0)=0,\ g(0)=0,\ f'(0)=1,\ g'(0)=C,\ \theta(0)=1,\ \phi(0)=1 \\ f'(\infty)\to 0,\ g'(\infty)\to 0,\ \theta(\infty)\to 0,\ \phi(\infty)\to 0 \end{array}\right\} \tag{14}$$

Journal of Chemistry and Technologies, 2025, *33*(2), 558-569

Wherein the relevant physical characteristics are described as

$$\left.\begin{aligned} &M=\frac{\sigma B_o^2}{\rho a},\ Nb=\frac{\tau_1 D_B\left(\varphi_w-\varphi_\infty\right)}{\nu},\ \mathrm{Pr}=\frac{\nu}{\alpha},\ \gamma=a\gamma_1,\ \delta=a\gamma_2,\\ &Nt=\frac{\nu D_T\left(T_w-T_\infty\right)}{\nu T_\infty},\ C=\frac{b}{a},\ Sc=\frac{\nu}{D_B},\ \lambda=\frac{1}{ak^*},\end{aligned}\right\} \quad (15)$$

The following are physically significant quantities

$$Cf_x=\frac{\tau_{wx}}{\rho u_w^2}\Rightarrow\left(\sqrt{\mathrm{Re}_x}\right)Cf_x=\left(1+\frac{1}{\beta}\right)f''(0) \quad (16)$$

$$Cf_y=\frac{\tau_{wy}}{\rho u_w^2}\Rightarrow\left(\sqrt{\mathrm{Re}_y}\right)Cf_y=\left(1+\frac{1}{\beta}\right)g''(0) \quad (17)$$

$$Nu_x=\frac{xq_w}{\kappa\left(T_w-T_\infty\right)}=-\frac{x\left(\frac{\partial T}{\partial z}\right)_{z=0}}{\kappa\left(T_w-T_\infty\right)}\Rightarrow Nu_x=-\left(\sqrt{\mathrm{Re}_x}\right)\theta'(0) \quad (18)$$

$$Sh=\frac{xq_m}{D_B\left(\varphi_w-\varphi_\infty\right)}=-\frac{x\left(\frac{\partial \varphi}{\partial y}\right)_{y=0}}{D_B\left(\varphi_w-\varphi_\infty\right)}\Rightarrow Sh=-\left(\sqrt{\mathrm{Re}_x}\right)\phi'(0) \quad (19)$$

Method of Solution via Finite element method

The finite element method, used in this study, is a versatile and powerful technique for addressing linear and nonlinear PDEs.It is a valuable tool for future research in fields like physics and mechanical engineering, and its applicability extends to a broad range of complex systems, indicating continued progress in these fields.The numerical solution for a flow, heat, and mass transfer problem is obtained using Mathematica, using the FEM. Equations derived from the model can be resolved through various numerical techniques, including the LU decomposition method and the Gauss elimination method, among others. When dealing with real numbers, it is crucial to consider the functional forms employed to approximate these real functions. The flow domain comprises a total of 20,001 nodes, which are systematically divided into 10,000 equally sized quadratic elements. Following the formulation of the element equations, we obtained a set of 80,004 nonlinear equations for further analysis. Upon applying the boundary conditions, the remaining system of nonlinear equations is solved numerically using the Gauss elimination technique, achieving a precision of 0.00001. Additionally, Gaussian quadrature is utilized to facilitate the resolution of integrals. The computational application for this methodology was developed using a programming language and executed on a desktop computer.

Program Code Validation

Table 1 compares the present numerical results with those of Nadeem et al. [45] for different permeability (λ) values at C = 0.5 and β = 1.0, neglecting Pr, Nt, Nb, Sc, γ, and δ effects. The close agreement between the results confirms the accuracy and robustness of the finite element method used in this study. This validation highlights the reliability of the computational approach compared to other numerical techniques. In the conclusion section, the key findings from Table 1 are summarized, reinforcing the validity of the present analysis.

Table 1

Validation of present Skin-friction coefficient along *x* and *y*-direction results with the results of Nadeem et al. [45]

M	Skin-friction coefficient results of this study along *x*	results of Nadeem [45]	Skin-friction coefficient results of this study in *y* direction	Results of Nadeem [45]
0.0	1.5254623545	1.5459	0.6354802807	0.6579
0.5	1.8152858292	1.8361	0.8058712823	0.8228
1.0	2.0567806876	2.0884	0.9455368265	0.9614

Results and Discussion

Using the same boundary conditions, the present mathematical model includes the Casson-Nanofluid to investigate the impacts of Cattaneo-Christov double diffusion, convective boundary conditions, magnetic fields, Brownian motion,

Journal of Chemistry and Technologies, 2025, *33*(2), 558-569

porous media, and thermophoresis. Three main nonlinear partial differential equations (PDEs) form this physical problem. The equations include concentration, energy, and motion. A collection of partial and non-linear ordinary differential equations (ODEs) is generated using similarity functions. They are solved using the Finite element technique to get precise answers considering the boundary conditions. We investigate many factors and evaluate how they affect the results. The results of the study may be viewed in Table 1 above. Figures 2 and 3 show the variations of the magnetic field parameter with respect to the main profile and the velocity profile,

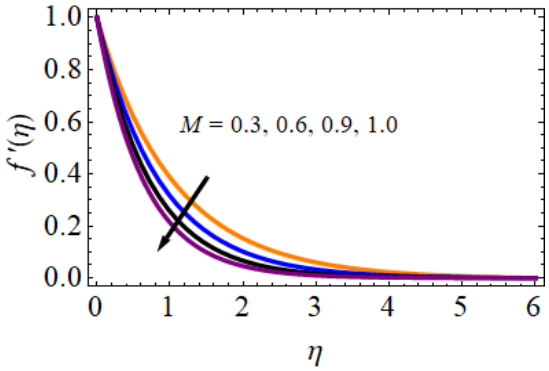

Fig. 2. Primary velocity profiles: *M* effect

respectively. Similar to the drag force, the Lorentz force develops as the magnitude of M increases. The Lorentz force stops motion and stops velocity profiles. Figures 4 and 5, respectively, show how the permeability parameter affects the primary and secondary velocity patterns. Numerical results show an inverse relationship between velocity profiles and porosity parameter K; a higher value for K results in a lower velocity profile. This is because as K increases, the momentum barrier layer becomes thinner due to the simultaneous growth of the porous layer. Figures 6 and 7 show how the primary and secondary velocity patterns are affected by

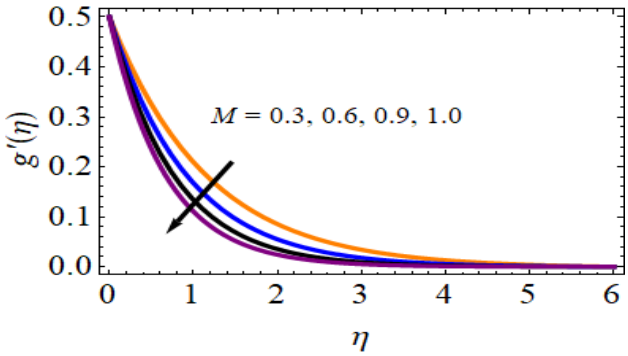

Fig. 3. Secondary velocity profiles

Figure 8 shows how the distribution of temperatures changes as a function of the Prandtl number. A higher Prandtl number is associated with a lower temperature field value and a thinner thermal layer. When the thermal diffusivity drops with increasing Prandtl number, a weaker temperature field and a smaller thermal layer are produced. Figures 9 and 10 show how Nb affects the temperature and concentration curves; in Figure 9, low Nb can perhaps improve the temperature profiles. Figure 9 shows these three processes, thermal boundary layer formation, and temperature increase. This rise is partly due to a higher Brownian motion parameter, lower viscous force, and stronger Brownian diffusion coefficient. Figure 10 shows that concentration decreases concomitantly with increasing *Nb*..Figures 11 and 12 correspondingly show, respectively, the impact of the thermophoresis parameter (Nt) on temperature and concentration profiles. The following profiles are presented below. The heat diffusion coefficient and the viscous force are used to calculate the thermophoresis parameter accurately. Given that viscous force and the thermophoresis parameter Nt are inversely correlated, increasing Nt leads to a decrease in viscous force while concurrently increasing the heat diffusion coefficient. These phenomena cause higher temperature values and higher nanoparticle density. The influence of the thermal relaxation time parameter is investigated in Figure 13 for the temperature distribution analysis. This result can be analyzed as follows: as the Thermal Relaxation Time Parameter increases, the temperature profiles decrease. The influence of mass relaxation time parameter (δ) on the temperature distributions can be inferred from Figure 14. The element concentration profiles become less sensitive as the parameter of mass relaxation time is increased. Figure 15 also shows that thermal Biot number (Bi) is directly proportional to the temperature distribution. The problem of the Thermal Biot number is referred to the analysis of the convection coefficient. Bi = 0 the results confirm the nonexistence of heat transfer through the wall. When the Thermal Biot number increases (Bi> 0), the heat transfer rate changes and the temperature distribution is higher. The temperature gradient in combination with mass transfer is capable of transferring mass from a region with a least solute concentration to a region with the highest solute concentration. Changes in the concentration distribution with the Schmidt number (Sc) are presented in Figure 16. Sc is the mass diffusivity to momentum diffusivity ratio where Sc = ν/ Dm. It is possible to determine the relative momentum and mass transfer by exploring the diffusion within the species' concentration boundary layer. As the Sc number increases, the mass diffusivity of the fluid

Journal of Chemistry and Technologies, 2025, *33*(2), 558-569

decreases, and hence the variance of the profiles of concentration decreases. Mass diffusivity and the Schmidt number (*Sc*) show an inverse connection wherein higher Schmidt number values match less concentration boundary layers. This results from the interplay of mass diffusivity with *Sc*.

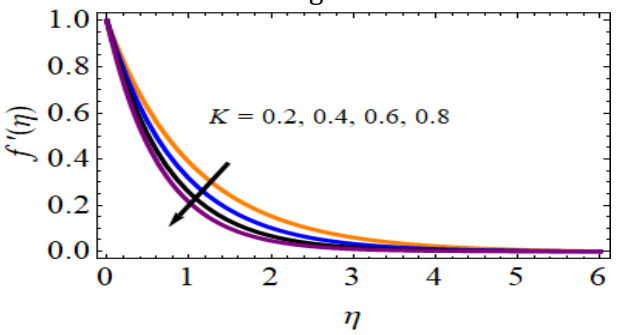

Fig. 4. *K* effect on primary velocity profiles

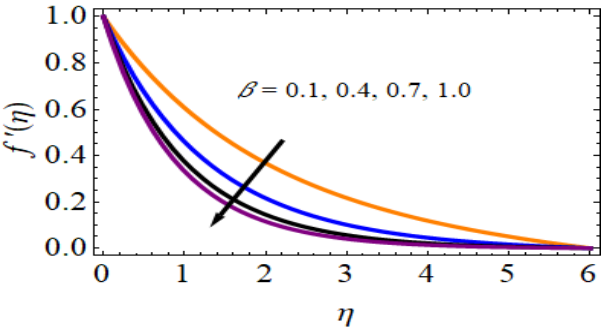

Fig. 6. Primary velocity profiles: effect of *β*

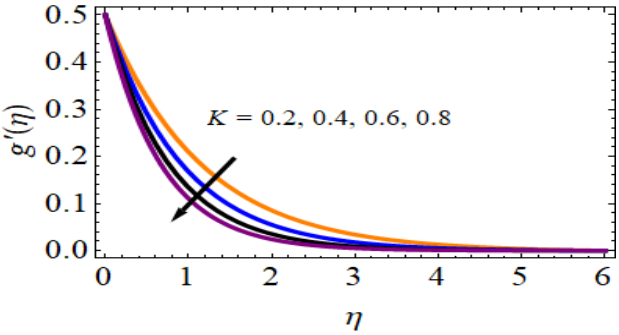

Fig. 5. Secondary velocity profiles: *K* effect

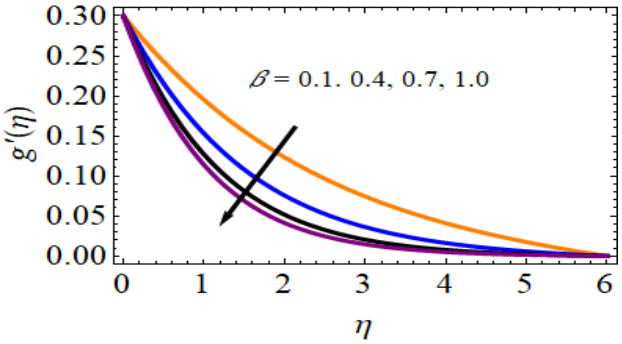

Fig. 7. Secondary velocity profiles: effect of *B*

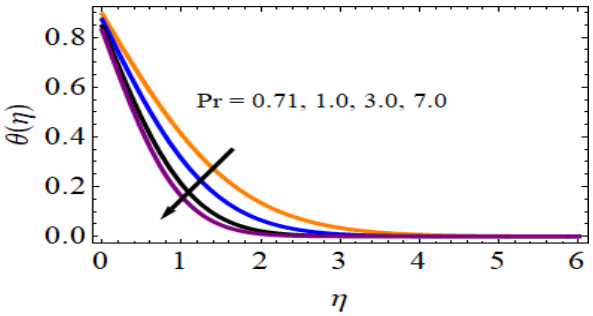

Fig. 8. Pr effect: temperature profiles

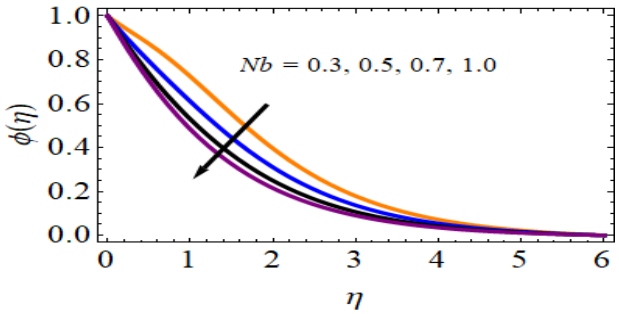

Fig. 10. Concentration profiles: effect of *Nb*

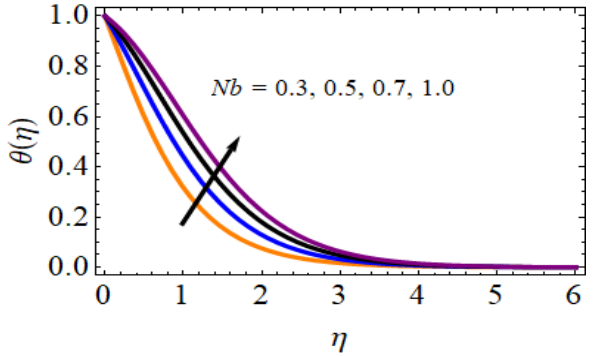

Fig. 9. Temperature profiles: effect of *Nb*

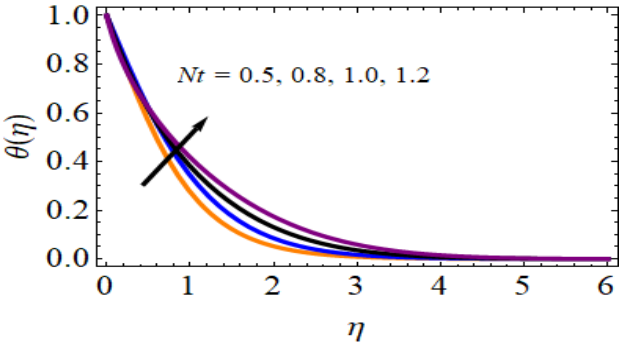

Fig. 11. Temperature profiles: effect of *Nt*

Table 4 shows that the Nusselt number was used to facilitate the derivation of numerical values of the heat transfer coefficient, which covers a wide range of Biot numbers (Bi), Prandtl numbers (Pr), Brownian motion parameters (Nb), thermal relaxation time parameters (ü) and thermophoresis parameters (Nt).As the Biot number (Bi) increases, the thermophoresis parameter (Nt) and Brownian motion parameter (Nb) also increase, and the heat transfer coefficient increases. However, when Pr and ü are large in magnitude, the opposite effect is obtained.

Journal of Chemistry and Technologies, 2025, *33*(2), 558-569

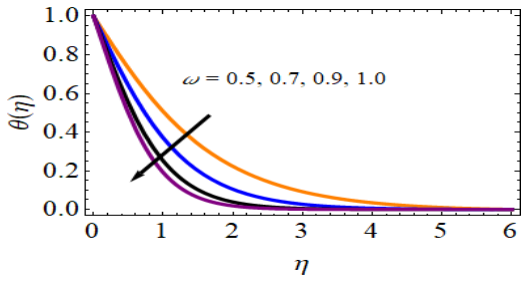

Fig. 12. ***Nt*** **effect: concentration profiles**

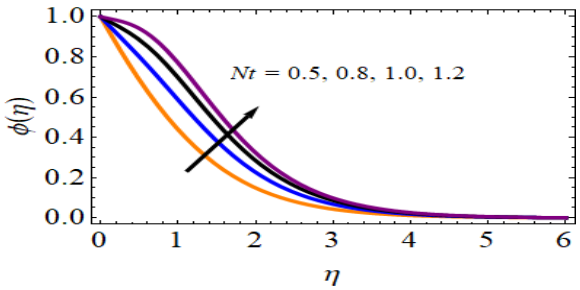

Fig. 13. ***Ω*** **effect: temperature profiles**

Table 5 summarizes the mass transfer coefficient densities for different values of Nb, Nt, Sc and δ as a function of Brownian motion, thermophoresis, mass relaxation time and Schmidt number parameters. Schmidt number, the Brownian motion parameter, and the mass relaxation time parameter negatively affect the heat transfer coefficient, but the thermophoresis parameter increases the heat transfer coefficient.

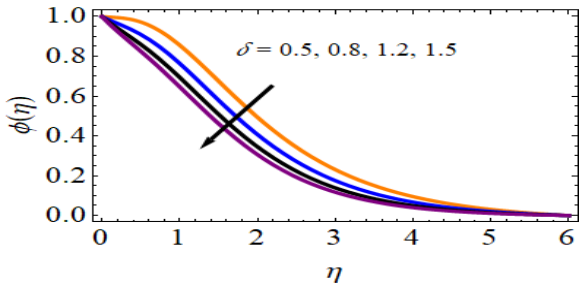

Fig. 14. ***δ*** **effect on concentration profiles**

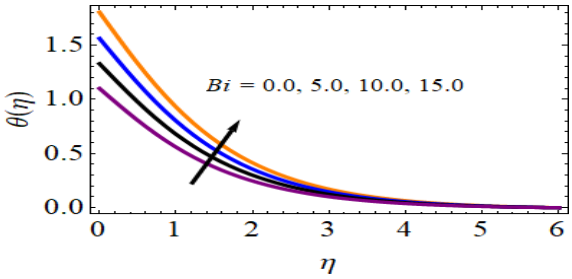

Fig. 15. ***Bi*** **effect on temperature profiles**

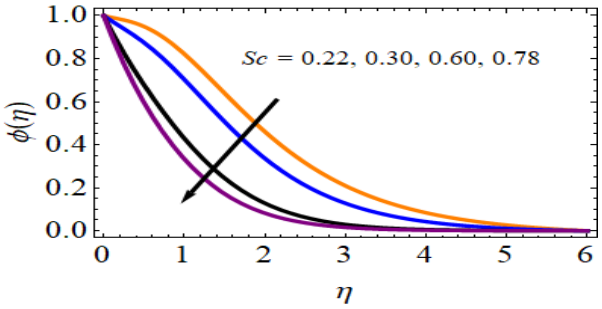

Fig. 16. ***Sc*** **effect on concentration profiles**

Tables 2 and 3 present the correlation between skin-friction coefficients (x and y directions) and key parameters. Positive correlations occur with Thermophoresis, Brownian motion, stretching ratio, and Biot number. Conversely, decreasing trends are observed for higher values of mass relaxation time, permeability, Casson fluid parameter, Prandtl number, thermal relaxation time, and Schmidt number. These results highlight the opposing influences of different physical factors on skin-friction behavior.One can visualize the results with the help of tables and graphs Tables 2, 3, and 4 show other parameters that can be determined from the obtained data including Sherwood number, Nusselt number, and local skin friction.

Table 2

Numerical values of Skin-friction coefficient calculated against velocity profiles.

M	*K*	*β*	*S*	Pr	*Nt*	*Nb*	*ω*	*Bi*	*Sc*	*δ*	Cf_x
0.3	0.2	0.1	0.5	0.71	0.5	0.3	0.5	5.0	0.22	0.5	3.6786691355
0.6											3.6480707627
0.9											3.6206671095
	0.4										3.6520721408
	0.6										3.6301856204
		0.4									3.6399580285
		0.7									3.6158928423
			1.0								3.7015708276
			1.5								3.7256062955
				1.00							3.6419952925

Continuation of Table 2

				3.00							3.6109872592
					0.8						3.6935087287
					1.0						3.7141438718
						0.5					3.6845629875
						0.7					3.7001598962
							0.7				3.6510756075
							0.9				3.6307652756
								10.0			3.7058287523
								15.0			3.7217658712
									0.30		3.6399875628
									0.78		3.6156812673
										0.8	3.6500585286
										1.2	3.6316542694

Table 3

Skin-friction coefficient numerical values resulting from secondary velocity profiles

M	*K*	*β*	*S*	Pr	*Nt*	*Nb*	*ω*	*Bi*	*Sc*	*δ*	Cf_y
0.3	0.2	0.1	0.5	0.71	0.5	0.3	0.5	5.0	0.22	0.5	2.3865760271
0.6											2.3507458762
0.9											2.3356628781
	0.4										2.3697607523
	0.6										2.3490697981
		0.4									2.3606961509
		0.7									2.3408560722
			1.0								2.4165750876
			1.5								2.4408237602
				1.00							2.3565608572
				3.00							2.3345366648
					0.8						2.4260686816
					1.0						2.4456701605
						0.5					2.4006650161
						0.7					2.4261006526
							0.7				2.3626456903
							0.9				2.3454892582
								10.0			2.4156019592
								15.0			2.4325676128
									0.30		2.3557608156
									0.78		2.3264501525
										0.8	2.3695661765
										1.2	2.3410656250

Table 4

Numerical values of heat transfer coefficient derived from temperature profiles

Pr	*Nt*	*Nb*	*ω*	*Bi*	Nu_x
0.71	0.5	0.3	0.5	5.0	1.8969046523
1.00					1.8523545085
3.00					1.8376851483
	0.8				1.9358072534
	1.0				1.9568687623
		0.5			1.9109768762
		0.7			1.9397687023
			0.7		1.8646576807
			0.9		1.8467075792
				10.0	1.9265067664
				15.0	1.9476009626

Table 5

Numerical values of mass transfer coefficient obtained from concentration profiles

Nt	*Nb*	*Sc*	*δ*	Sh_x
0.5	0.3	0.22	0.5	2.5670625209
0.8				2.6059263692
1.0				2.6359692515
	0.5			2.5966529081

Continuation of Table 5

0.7			2.6265902523
	0.30		2.5209686253
	0.78		2.4912342325
		0.8	2.5378681854
		1.2	2.5140746732

Conclusions

In our recent research endeavor, we have meticulously tackled the analytical challenge of numerically solving linear differential equations that govern the magneto-hydrodynamic Casson-Nanofluid flow over a stretching sheet. By employing advanced mathematical techniques and leveraging the expertise of our team, we have successfully navigated the complexities of this intricate problem, ultimately contributing to a deeper understanding of fluid dynamics in the context of nanofluids and magnetic fields. The results of magnetic field, thermophoresis, porous substrate, Brownian motion, and Cattaneo Christov double diffusion are considered in this investigation. We study the x- and y-dimensional velocity components, temperature and concentration profiles, by the Finite element method, as functions of various parameters. Particularly, we examine effects of different values on the key parameters. This study has led to the following final conclusions:

- The values of thermophoresis and Brownian motion parameters are given, with the Biot parameters increasing as the temperature profiles increase, and the Prandtl parameters and thermal relaxation times decreasing.
- The primary and secondary velocity patterns decrease as the Casson fluid, permeability, and magnetic field parameters rise.
- Concentration profiles decrease with increasing Schmidt number, with increasing mass relaxation time and Brownian motion parameters; the trend is reversed with increasing thermophoresis parameter.
- The results derived from the present methodology are outstanding and consistent with the conclusions of Nadeem et al. [45] in the absence of Casson fluid and double Cattaneo-Christov diffusion effects.

References

[1] Nadeem, S., Lee, C. (2016). Series solution of magneto-hydrodynamic boundary layer flow over bi-directional exponentially stretching surfaces, *J. Braz. Soc. Mech. Sci. Eng., 38*(2), 443–453. https://doi.org/10.1007/s40430-015-0344-2

[2] Sadiq, M.A., Nadeem, S. (2015). Unsteady MHD boundary layer flow of a couple stress nano fluid over a stretching/shrinking surface with convective boundary condition, *J. Comput. Theor. Nanosci., 12*(11), 4408–4414.

[3] Akbar, N., Khan, Z., Nadeem, S., Khan, W. (2016). Double-diffusive natural convective boundary-layer flow of a nanofluid over a stretching sheet with magnetic field *Int. J. Numer. Methods Heat Fluid Flow, 26*(1), 108–121.

[4] Hussain, S., Rasheed, K., Ali, A., Vrinceanu, N., Alshehri, A., Shah, Z. (2022). A sensitivity analysis of MHD nanofluid flow across an exponentially stretched surface with non-uniform heat flux by response surface methodology. *Sci. Rep., 12*, 18523. https://doi.org/10.1038/s41598-022-22970-y

[5] Ali, A., Khan Marwat, D.N., Ali, A. (2022). Analysis of flow and heat transfer over stretching/shrinking and porous surfaces. *J. Plast. Film Sheeting Plast. Film Sheeting 38*(1), 21–45. https://doi.org/10.1177/87560879211025

[6] Hsiao, K.L. (2016). Stagnation electrical MHD nanofluid mixed convection with slip boundary on a stretching sheet. *Appl. Therm. Eng. 98*, 850–886

[7] Awais, M., Hayat, T., Ali, A., Irum, S. (2016). Velocity, thermal and concentration slip effects on a magneto-hydrodynamic nanofluid flow. *Alex. Eng. J., 55*(3), 2107–2114.

[8] Khashiie, N.S., Arifin, N.M., Pop, I., Nazar, R., Hafidzuddin, E.H., Wahi, N. (2020). Three-dimensional hybrid nanofluid flow and heat transfer past a permeable stretching/shrinking sheet with velocity slip and convective condition. *Chin. J. Phys., 66*, 157–171. https://doi.org/10.1016/j.cjph.2020.03.032

[9] Makinde, O.D., Aziz, A. (2011). Boundary layer flow of a nanofluid past a stretching sheet with a convective boundary condition. *Int. J. Therm. Sci. 50*(7), 1326–1332.

[10] Khan, W.A., Pop, I. (2010). Boundary-layer flow of a nanofluid past a stretching sheet. *Int. J. Heat Mass Transf., 53*, 2477–2483.

[11] Cattaneo, C. (1948). Sulla conduzione del calore, AttiSemin. *Mat. Fis. Univ. Modena Reggio Emilia, 3*, 83–101.

[12] Ciarletta, M., Straughan, B. (2010). Uniqueness and structural stability for the Cattaneo-Christov equations, *Mech. Res. Commun., 37*(5), 445–447.

[13] Mustafa, M. (2015). Cattaneo-Christov heat flux model for rotating flow and heat transfer of upper-convected Maxwell fluid, *AIP Adv., 5*(4), 047109. https://doi.org/10.1063/1.4917306

[14] Straughan, B. (2010). Thermal convection with the Cattaneo-Christov model, Int. *J. Heat Mass Transfer, 53*(1), 95–98.

[15] Han, S., Zheng, L., Li, C., Zhang, X. (2014). Coupled flow and heat transfer in viscoelastic fluid with Cattaneo-Christov heat flux model, *Appl. Math. Lett., 38*, 87–93.

[16] Hayat, T., Khan, M.I., Farooq, M., Alsaedi, A., Waqas, M., Yasmeen, T. (2016). Impact of Cattaneo-Christov heat flux model in flow of variable thermal conductivity fluid over a variable thicked surface, *Int. J. Heat Mass Transfer, 99*, 702–710.

[17] Hayat, T., Khan, T., Farooq, M., Yasmeen, T., Alsaedi, A. (2016). Stagnation point flow with Cattaneo-Christov heat flux and homogeneous-heterogeneous reactions, *J.*

Mol. Liq., 220, 49–55. https://doi.org/10.1016/j.molliq.2016.04.032

[18] Farooq, M., Khan, M.I., Waqas, M., Hayat, T., Alsaedi, A., Khan, M.I. (2016). MHD stagnation point flow of viscoelastic nanofluid with non-linear radiation effects, *J. Mol. Liq., 221*, 1097–1103.

[19] Hayat, T., Bashir, G., Waqas, M., Alsaedi, A. (2016). MHD flow of Jeffrey liquid due to a nonlinear radially stretched sheet in presence of Newtonian heating, *Results Phys., 6*, 817–823.

[20] Afzal, K. Aziz, A. (2016). Transport and heat transfer of time dependent MHD slip flow of nanofluids in solar collectors with variable thermal conductivity and thermal radiation, *Results Phys., 6*, 746–753.

[21] Gundagani, M., Babu, N.V.N., Gadially, D. S. Bhati, M. Sanjay, Ch., Nirmala Kasturi, V.. (2024). Study of Nano-Powell-Erying fluid flow past a porous stretching sheet by the effects of MHD, thermal and mass convective boundary conditions. *J. Umm Al-Qura Univ. Eng. Archit.* https://doi.org/10.1007/s43995-024-00056-2

[22] Murali, G., Deepa, G., Kasturi, N. V., Poornakantha, T. (2023). Joint effects of thermal diffusion and diffusion thermo on MHD three dimensional nanofluid flow towards a stretching sheet, Mathematical models in engineering,9(4),130143,https://doi.org/10.21595/mme.2023.23590.

[23] Gundagani, M., Mamidi, L.P., Tanuku, P.K. (2024). Finite element solutions of Double diffusion effects on three-dimensional MHD Nano-Powell-Erying fluid flow in presence of thermal and mass Biot numbers. *J. Eng. Appl. Sci., 71*, 9. https://doi.org/10.1186/s44147-023-00347-w

[24] Murali, G., Babu, N.V.N. (2023). Convective MHD Jeffrey Fluid Flow Due to Vertical Plates with Pulsed Fluid Suction:A Numerical Study, *Journal of computational applied mechanics, 54*(1), 36–48. doi: 10.22059/JCAMECH.2023.351326.773.

[25] Mebarek-Oudina, F., Dharmaiah, G., Rama Prasad, J. L., Vaidya, H., Kumari, Thermal, M. A. (2025). Flow Dynamics of Magnetohydxrodynamic Burgers' Fluid Induced by a Stretching Cylinder with Internal Heat Generation and Absorption, *International Journal of Thermophysics, 25,* 100986. https://doi.org/10.1016/j.ijft.2024.100986

[26] Kirubaharan, D.R., Subhashini, A.D., Murali, G. (2024). Study of Three Dimensional Casson-Nanofluid Flow due to a Linear Porous Stretching Sheet in the Presence of Double Diffusion Effects, *Advances in Systems Science and Applications*, *24*(3), 90–103. https://doi.org/10.25728/assa.2024.2024.03.1539

[27] Murali, G., Deepa, G., Venkata Madhu, J., Nirmala Kasturi, V., Bhati, S.M., Narendra Babu, N. (2025). Three Dimensional Chemically Reacting Oldroyd-B Fluid + Nanofluid Flow in Presence of Thermophoresis and Brownian Motion Effects, *Discontinuity, Nonlinearity, and Complexity*, *14*(2), 373–388. https://doi.org/10.5890/DNC.2025.06.010

[28] Tanuku, P.K., Mamidi, L.P., Gundagani, M. (2024). Modelling and analysis of three-dimensional chemically reacting, radiating Casson-nanofluid flow: thermophoresis and Brownian motion effects, *Acta Polytechnica*, *64*(5), 455–463. https://doi.org/10.14311/AP.2024.64.0455

[29] Murali, G., Lakshmi, P., Amarnath, M. (2025). Three-dimensional MHD flow of a radiative Eyring–Powell nanofluid: Exploring Hall effects and heat transfer. *Theor Math Phys., 223*, 1070–1086. https://doi.org/10.1134/S0040577925060170

[30] Murali, G., Venkata Madhu, J., Deepa, G. (2025). Hall current and MHD impacts on a 3D Maxwell nanofluid flow across a porous stretching surface. *Theor Math Phys* 223, 899–914. https://doi.org/10.1134/S0040577925060030

[31] Anil Kumar, M., Mebarek-Oudina, F., Mangathai, P., Shah, N. A., Vijayabhaskar, N., Venkatesh, Ch., Fouad, Y. (2025). The Impact of Soret Dufour and Radiation on the Laminar Flow of a Rotating liquid past a Porous plate via Chemical Reaction, *Modern Physics Letters B, 39*(10), 2450458. https://doi.org/10.1142/S021798492450458X

[32] Rajesh, V, Sheremet, M. (2023). Free Convection in a Square Ternary Hybrid Nanoliquid Chamber with Linearly Heating Adjacent Walls. *Nanomaterials, 13*(21). https://doi.org/10.3390/nano13212860

[33] Khan, Y, Majeed, AH, Shahzad H. (2022). Numerical Computations of Non-Newtonian Fluid Flow in Hexagonal Cavity With a Square Obstacle: A Hybrid Mesh–Based Study. *Front Phys., 10*. https://doi.org/10.3389/fphy.2022.891163

[34] F. Mebarek-Oudina, M. Bouselsal, N. Biswas, H. Vaidya, K. Ramesh, Heat transfer in a zigzag wall cavity and different obstacles filled with MgO-SWCNT/water hybrid nanofluids, Modern Physics Letters B, (2025) 2550163. https://doi.org/10.1142/S0217984925501635

[35] Raza, J., Mebarek-Oudina, F., Ali, H., Sarris, I. E. (2024). Slip effects on Casson Nanofluid over a Stretching sheet with activation energy: RSM Analysis, *Frontiers in Heat and Mass Transfer, 22*(4), 1017–1041. https://doi.org/10.32604/fhmt.2024.052749

[36] Ould Said, B., Mebarek-Oudina F., Medebber, M. A. (2024) Magneto-hydro-Convective Nanofluid flow in Porous Square Enclosure, *Frontiers in Heat and Mass Transfer, 22*(5), 1343–1360. https://doi.org/10.32604/fhmt.2024.054164

[37] Ramesh, K. Mebarek-Oudina, F. Souayeh, B. (2023). *Mathematical Modelling of Fluid Dynamics and Nanofluids*, 1st edition, CRC Press (Taylor & Francis). https://doi.org/10.1201/9781003299608

[38] Mebarek-Oudina, F. (2025). *CFD Simulation: Thermo-Fluids and Nanofluids in Engineering and Biomedicine*, 1st edition, De-Gruyter. https://doi.org/10.1515/9783111405094

[39] Mezaache, A., Mebarek-Oudina, F., Vaidya, H., Fouad, Y. (2024). Heat Transfer Analysis of Nanofluid Flow with Entropy generation in a Corrugated Heat Exchanger Channel Partially filled with Porous Medium. *Heat Transfer, 53*(8), 46254647. https://doi.org/10.1002/HTJ23149.

[40] Gupta, T., Pandey, A. K., Kumar, M. (2023). Effect of Thompson and Troian slip on CNT-Fe_3O_4/kerosene oil hybrid nanofluid flow over an exponential stretching sheet with Reynolds viscosity model. *Mod. Phys. Lett. B,* 2350209. doi:10.1142/S0217984923502093

[41] Poornakantha, T., Laksmiprsanna, M., Murali, G. (2025). Modelling and Analysis of Three-Dimensional Maxwell-Nanofluid Flow over a Bi-Directional Stretching Surface in the Presence of a Magnetic Field. *International Journal for Engineering Modelling, 38*(1), 53–72. https://doi.org/10.31534/engmod.2025.1.ri.04d.

[42] Sivaiah, S., Gundagani, M., Karanamu, M. P. (2012). Analysis of Heat and Mass Transfer Effects on an Isothermal Vertical Oscillating Plate. *Walailak J. Sci. Tech., (WJST), 9*(4), 407–415.

[43] Murali, G., Venkata Madhu, J., Deepa, G., Suresh, P., Nagaraju, B. (2025). Three-Dimensional Oldroyd-B Fluid Flow Past a Stretching Surface with Magnetic Field, Nanofluid Particles and Cattaneo-Christov Double Diffusion Effects, *Johnson Matthey Technology Review, 69*(2), 299–320. https://doi.org/10.1595/205651325X17375408788409 .

[44] Gundagani, M., Javvaji, V. Gadipalli, D. Pallerla, S. Al-Mdallal Q., Bhati, S. (2025). A Numerical Study on MHD 3-D Casson-Nanofluid Flow Past an Exponentially Stretching Sheet with Double Cattaneo-Christov Diffusion Effects, *Rev. int. métodos numér. cálc. diseño ing*., *41*(2), 21.

[45] Nadeem, S., Haq, R. U., Akbar, N. S., Khan, Z. H. (2013). MHD three-dimensional Casson fluid flow past a porous linearly stretching sheet. *Alexandria Engineering Journal, 52*(4), 577–582. https://doi.org/10.1016/j.aej.2013.08.005 .